High Multiplicity pp and pA Collisions: The Hydrodynamics at its Edge

Edward Shuryak and Ismail Zahed

Department of Physics and Astronomy,
Stony Brook University,
Stony Brook, NY 11794, USA

(Dated: February 24, 2022)

With growing multiplicity, the pp and pA collisions enter the domain where the macroscopic description (thermodynamics and hydrodynamics) becomes applicable. We discuss this situation, first with simplified thought experiments, then with some idealized representative cases, and finally address the real data. For clarity, we don't do it numerically but analytically, using the Gubser solution. We found that the radial flow is expected to increase from central AA to central pA, while the elliptic flow decreases, with higher harmonics being comparable. In the second part of the paper we approach the problem from the opposite side, using a string-based Pomeron model. We extensively study the magnitude and distribution of the viscous corrections, in Navier-Stokes and Israel-Stuart approximations, ending with higher gradient re-summation proposed by Lublinsky and Shuryak. We found those corrections growing, from AA to pA to pp, but remaining at the manageable size even in the last case.

I. INTRODUCTION

High energy heavy ion collisions are theoretically treated very differently from pp and pA ones. While the former are very well described using macroscopic theories – thermodynamics and relativistic hydrodynamics – the latter are subject to what we would like to call the "pomeron physics", described with a help of microscopic dynamics in terms of (ladders of) perturbative gluons, classical random gauge fields, or strings. The temperature and entropy play a central role in the former case, and are not even mentioned or defined in the latter case.

The subject of this paper is the situation when these two distinct worlds (perhaps) meet. In short, the main statement of this paper is that specially triggered fluctuations of the pp and pA collisions of particular magnitude should be able to reach conditions in which the macroscopic description can be nearly as good as for AA collisions. While triggered by experimental hints at LHC to be discussed below, this phenomenon has not yet been a subject of a systematic study experimentally or theoretically, and is of course far from being understood. So on onset let us enumerate few key issues to be addressed.

- How do the thermodynamical and hydrodynamical (viscosities, relaxation time etc) quantities scale with the change in the system size R and the multiplicity N? What are the criteria for macroscopic (hydrodynamical) behavior ?

- What are the consequences of the fact that the sQGP phase of matter is approximately scale invariant ?

- Do high multiplicity pp and pA collisions in which the (double) "ridge" has been recently observed at LHC [6–8] fit into the hydrodynamical systematics tested so far for AA collisions?

- What is the expected magnitude of the radial flow in pp and pA collisions, and how is it related to that in AA? What are the freezeout conditions in these new explosive systems?

- How do amplitudes of the second and higher angular harmonics v_n scale with n,R and η/s? In which p_t region do we expect hydrodynamics to work, and for with v_n?

The major objective of the heavy ion collision program is to create and study properties of a new form of matter, the Quark-Gluon Plasma. Among many proposed signatures proposed in [2], the central role is played

by production of macroscopic fireball of such matter, with the subsequent collective explosion described by the relativistic hydrodynamics. Its observable effects are include radial and elliptic flow, supplemented by higher moments $v_m, m > 2$. At RHIC and LHC the AA collisions has been studied in detail by now, with multiple measured dependences, with excellent agreement with hydrodynamics in a wide domain, for $n < 7$ and in the range of $p_t < 3\,GeV$.

Let us start with a very generic discussion of applicability of hydrodynamics. The basic condition is that the system's size R should be much larger than microscopic scales such as e.g. the correlation lengths or the inverse temperature T^{-1}. The corresponding ratio is one small parameter

$$\frac{1}{TR} \approx \mathcal{O}(1/10) \ll 1 \tag{1}$$

where the value corresponds to well studied central AA collisions. Another important small parameter which we seem to have for strongly coupled Quark-Gluon Plasma (sQGP) is the *viscosity-to-entropy-density ratio*

$$\frac{\eta}{s} = 0.1..0.2 \ll 1 \tag{2}$$

This tells us that viscous scale – the mean free path in kinetic terms – is additionally suppressed compared to the micro scale $1/T$ by strong interaction in the system. The *product* of both parameters appearing in expressions (to be specified below) suggests that one can hope to apply hydrodynamics with about percent accuracy.

The reason why the fireballs produced in AuAu collisions at RHIC and PbPb at LHC behaves macroscopically is related to the *large size* of the colliding nuclei used. Yet smaller size systems occurring in pp or pA should also be able to do so, provided certain conditions are met. Let us thus start to define such a comparison, starting with our *thought experiment 0*, in which two systems (see a sketch in Fig.1) A and B have the same local quantities – temperatures, viscosities and the like – but different sizes $R_A > R_B$. (For example, think of AuAu and CuCu collisions at the same collision energy, as in experiments done at RHIC.) The equations of *ideal* hydrodynamics

$$\partial_\mu T^{\mu\nu} = 0 \tag{3}$$

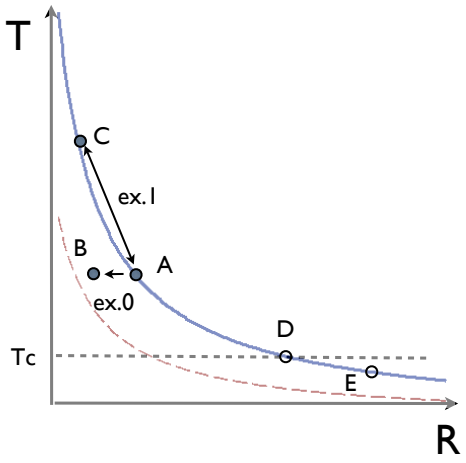

FIG. 1: (color online) Temperature T versus the fireball size R plane. Solid blue line is the adiabate $S = const$, approximately $TR = const$ for sQGP. Example 0 in the text corresponds to reducing R, moving left $A \to B$. Example 1 is moving up the adiabate $A \to C$. Example 2 corresponds to adiabatic expansion, such as $A \to E$,$C \to E$. If in reality C corresponds to pA, the freezeout occurs at the earlier point D.

include derivatives linearly and therefore simultaneous rescaling of the size and the time $x^\mu \to \lambda x^\mu$ does not change them. So, *ideal* hydrodynamics will produce the same solution for fireball of any size, provided other parameters are unchanged. Yet the viscous terms have more gradients, and thus there is no such symmetry. Going from a large AA fireball to smaller $pA..pp$ systems would increases the role of visous terms (scaled as powers of $1/R$) , eventually invalidating hydrodynamics. (The boundary of which is shown in Fig.1 by red long-dashed line.)

However if local quantities such as T are changed as well, as is indeed the case in experimental conditions we will discuss, the conclusion may change. Consider instead the *thought experiment 1*, in which we compare two systems on the same adiabate A and C. For conformally invariant sQGP – such as exists in the $\mathcal{N}$=4 supersymmetric theory without running coupling – $S \sim (TR)^3 = const$ and the points A, C are related by the scale transformation

$$R_A/R_C = \xi, T_A/T_C = \xi^{-1} \tag{4}$$

If the scale transformation is a symmetry, all densities – e.g. the energy densities – scale with the naive dimensional powers of the temperature $\epsilon/T^4 \sim const$, viscosities do the same. Thus *the absolute scale plays no role*. A small (but hotter) plasma ball C will behave exactly in the same way as the large (but cooler) A, provided all dimensionless quantities like TR or total entropy/multiplicity are held constant.

Let us now proceed to the *thought experiment 2*, which is the same as above but in QCD, with a running coupling. In the sQGP regime it leads to (very small, as lattice tells us) running of s/T^3, of (unknown) running of η/T^3 etc. The most dramatic effect is not the running coupling *per se*, but the lack of supersymmetry, which induces chiral/deconfinement phase transition out of the sQGP phase at $T = T_c$. The end of the sQGP explosion D thus has an *absolute scale*, not subject to scale transformation!

So let us consider two systems A,C of the same total entropy/multiplicity, initiated in sQGP with conditions related by scale transformation and left them explode. The sQGP evolution would be related by nearly the same set of intermediate states (modulo running coupling) till $T \approx T_c$, after which they go into the "mixed" and hadronic stages, which are *not* even close to be scale invariant! Thus the result of the explosions are not the same. In fact the smaller/hotter system will have an advantage over the larger/cooler one, since it has *larger* ratio between the initial and final scales T_i/T_f.

(In the language of holographic models the scale is interpreted as the 5-th coordinate x^5, and evolution is depicted as gravitational falling of particles,strings, fireballs etc toward the AdS center. The ratio of the scales is the distance travelled in the 5-th coordinate: thus in this language two systems fall similarly in the same gravity, but smaller system starts "higher" and thus got larger velocity at the same level given by T_c.)

The hydro expansion does not need to stop at the phase boundary D. In fact large systems, as obtained in central AA collisions are known to freezeout at $T_f < T_c$, down to 100 MeV range (and indicated in the sketch by the point E. However small systems, obtained in peripheral AA or central pA seem to freezeout at D, as we will show at the end of the paper.

Short summary of these thought experiments: not only one expects hydro in the smaller/hotter system to be there, it should be similar to the one in larger/cooler system, due to approximate scale invariance of sQGP. Furthermore, in fact smaller systems are expected to produce *stronger* hydro flow, as they evolve "longer" (not in absolute but in dimensionalless time).

If one wants to make comparison along such lines, the question is how one can increase the temperature of the system in practice. One obvious way to do so is to increase the collision energy: taking a pair of lighter nuclei $A'A'$ at LHC one can compare it to collision of heavier nuclei AA at RHIC tuning the energy so that the multiplicity and centrality of the collisions be the same, reproducing our thought experiment 2. Yet energy dependence of multiplicity is very slow, RHIC and LHC have different detectors etc: so it is not very practical. Another option is to rely on rare fluctuations, selecting events with a larger entropy/multiplicity. This is very expensive[30], but this is what is done in practice.

Let us now briefly outline the history of the subject of collective flow effects in pp collisions. The radial flow effects in were searched for in the minimum-bias pp collisions at CERN ISR more than 30 years ago by one of us [3], with negative results. Indications for some radial flow have been found in specially triggered $\bar{\text{p}}$p collisions by the FERMILAB MINIMAX experiment [4], but the data remained inconclusive and, more importantly, the magnitude of the flow was small, below of what the full-fledged hydro would give. (We are not aware of any actual comparison with these data.)

With the advent of the LHC era of extremely high luminocities and short-time detector capabilities, a hunt for strong fluctuations in the parton multiplicity became possible. Already during the very first run of LHC in 2010, the CMS collaboration was able [5] to collect sufficient sample of high multiplicity *pp* collisions occurring with the probability $\sim 10^{-6}$. CMS found the "ridge" correlation in the highest multiplicity bins, an angular correlation in the azimuthal angle between two particles at $\Delta\phi < 1$ which extends to large rapidity range $|\Delta y| \geq 4$. More recently the same phenomenon was seen in pPb collisions as well, now by the CMS [6], ALICE [7] and ATLAS [8] collabora-

tions, as well as by PHENIX [9] in dAu collisions at RHIC. Larger number of "participant nucleons" and higher average multiplicity substantially weaken the cost of the trigger: the "ridge" is seen at the trigger level of few percents higher multiplicity events. It is shown in those works that in pp and pA collisions, the same threshold in terms of multiplicity is needed to start showing the "ridge".

Angular correlations naturally appear in a hydrodynamical explosion of a non-azimuthally symmetric objects. The spatial shape is then translated to momentum space and is observed. For example, in the comments on the CMS discovery written by one of us [10] it was illustrated by a string placed outside of an (axially symmetric) stick of explosive. While the basic wind blowing is isotropic in ϕ, an extra string may move in a preferred direction. In central AA collisions it is similar to that. A symmetric explosion has perturbations in the form of localized "hot spots". But in general, any sufficiently deformed initial collisions for the fireball would be sufficient to create ridge-like correlations.

Furthermore, the subtraction of the so called "back-to back recoil" (a peak at $\phi \sim \pi$) (evaluated from some perturbative (e.g. HIJING) or color glass models [29] or seen experimentally in smaller multiplicity bins) reveals that a ridge is "doubled on the away side. The remaining correlation function is found to be [7, 8] nearly symmetric with $x \to -x, \phi \to \pi - \phi$. Furthermore, the *second* angular harmonics completely dominate the correlator – unlike the central AA, in which the strongest harmonics is the third. The first attempts to describe this phenomenon hydrodynamically are qualitatively consistent with these data. For the pA case, it is Ref. [11], which starts from Glauber-inspired initial conditions similarly to what is done in the AA case.

A nucleon propagating through the diameter of the Pb nucleus "wounds" up to 20 nucleons. Similar number of "wounded nucleons" and multiplicity can be found for very peripheral PbPb collisions. Since these two systems have different transverse area, they approximately correspond to our "thought experiment 2" (modulo different shape, which can be accounted for, see below).

The objective of this paper is to extend hydrodynamical studies, using instead of a complicated "realistic models" with huge number of details and heavy numerics (the "event-by-event" hydrodynamics) an *analytic* approach. As we will see, this will allow us to focus on generic dependences of the predictions on the parameters of the problem.

The structure of the paper is as follows. In the next section we discuss the radial flow using Gubser's solution. After putting AA,pA,pp representative cases into common dimensionless units, we see that they are in fact not so far from thought experiments just discussed. We will then study viscous effects, from the Navier-Stokes term, to Israel-Stuart equations and Lublinsky-Shuryak higher gradient re-summation in section II D. We found an artifact of Gubser solution –large corrections on the space-like part of the freeze out surface, but other than that all viscous effects seem to be reasonabley under control, in all cases considered. We then turn to the harmonics of the flow v_m in the next section, with m=2,3 and higher. We start with "acoustic damping" formula, outlying dependence on the parameters, and then proceed to solving the equations for Gubser flow perturbations in AA,pA and pp cases. The last section is devoted to comparison to the experimental data. Only very recently spectra of the identified secondaries for high-multiplicity pA had allowed to confirm our main point: the increase of the radial flow, and even determine more quantitatively the freeze out conditions.

II. HYDRODYNAMICS OF THE RADIAL FLOW

A. Ideal hydrodynamics and the Gubser's flow

Since we are interested in comparison of different systems, it is important not to have too many details which can be different and induced some variations in both. In particularly, one should keep the matter distribution of the same shape. It is sufficient for this purpose to use a relatively simple analytic solution found by Gubser [18], see also [19]. This solution has two symmetries: the boost-invariance as well as the axial symmetry in the transverse plane.

It is obtained via special conformal transformation, and therefore, the matter is required to be conformal, with the EOS

$$\epsilon = 3p = T^4 f_* \tag{5}$$

where the parameter $f_* = 11$ is fitted to reproduce the lattice data on QGP thermodynamics (not too close to T_c).

The coordinate sets used are either the usual proper time -spatial rapidity - transverse radius - azimuthal angle $(\bar{\tau}, \eta, \bar{r}, \phi)$ set with the metric

$$ds^2 \;=\; -d\bar{\tau}^2 + \bar{\tau}^2 d\eta^2 + d\bar{r}^2 + \bar{r}^2 d\phi^2, \tag{6}$$

or the comoving coordinates we will introduce a bit later.

The shape of the solution is fixed, and the absolute scale is introduced by a single parameter q with dimension of the inverse length. We call the dimensionful variables $\bar{\tau}, \bar{r}$ with the bar, which disappears as we proceed to dimensionless variables

$$t = q\bar{\tau}, \;\; r = q\bar{r} \tag{7}$$

In such variable there is one single solution of ideal relativistic hydrodynamics, which for the transverse velocity and the energy density reads

$$v_\perp(t,r) \;=\; \frac{2tr}{1+t^2+r^2} \tag{8}$$

$$\frac{\epsilon}{q^4} \;=\; \frac{\hat{\epsilon}_0 2^{8/3}}{t^{4/3}\left[1+2(t^2+r^2)+(t^2-r^2)^2\right]^{4/3}}$$

The specificity of the system considered is reduced to a single dimensionalless parameter

$$\hat{\epsilon}_0 = \tag{9}$$

related to macro-to-micro ratio (1) or multiplicity, plus of course different freezeouts to which we turn shortly.

Let us crudely map the AA, pA and pp collisions to these coordinates, guessing the scale factors in fm to be

$$q_{AA}^{-1} = 4.3, \;\; q_{pA}^{-1} = 1, \;\; q_{pp}^{-1} = 0.5 \tag{10}$$

The energy density parameter can be related to the entropy-per-rapidity density of the solution

$$\hat{\epsilon}_0 = f_*^{-1/3}\left(\frac{3}{16\pi}\frac{dS}{d\eta}\right)^{4/3} \tag{11}$$

which in turn is mapped to multiplicity density per unit rapidity

$$\frac{dS}{d\eta} \approx 7.5\;\frac{dN_{ch}}{d\eta} \tag{12}$$

defined at freezeout. We use for central LHC AA=PbPb collisions

$$dN_{ch}^{AA}/d\eta = 1450 \tag{13}$$

The pp and pA data are split into several multiplicity bins: for definiteness, we will refer to one of them in the CMS set, with the (corrected average) multiplicity $N_{ch} = 114$ inside $|\eta| < 2.4$ and $p_t > 0.4\,GeV$ acceptance. We thus take

$$dN_{ch}^{pA}/d\eta = dN_{ch}^{pp}/d\eta = 1.6\;\frac{114}{2*2.4} \tag{14}$$

where the factor 1.6 approximately corrects for the unobserved $p_t < 0.4\,GeV$ region. Similarly the energy parameters are fixed for each multiplicity bin.

(For clarity: our thought experiments 1 and 2 of the Introduction assumed the *same* values of $\hat{\epsilon}_0$ for points A and C, thus the same solution. Now we compare central AA and some representative bins of pA and pp, which have parameters and correspond to $different$ adiabatic curves.)

The expression for transverse flow (8) does not depend on $\hat{\epsilon}_0$ though, and all one needs to do to calculate the radial flow is to define the freezeout surfaces. Such a map is shown on the t, r plot in Fig.2, in which we, for now, selected the same "average" freezeout temperature $T_f = 150\,MeV$ (to be modified later). Hydrodynamics is valid between the (horizontal) initial time lines and the contours of fixed freeze out temperature T_f, shown by thicker solid line, at which the particle decouple and fly to the detector. The spectra should be calculated by the standard Cooper-Fry formula

$$\frac{dN}{d\eta dp_\perp^2} \sim \int p^\mu d\Sigma_\mu \,\exp\left(-\frac{p^\mu u_\mu}{T_f}\right) \tag{15}$$

in which Σ_μ is the freeze out surface, on which the collective velocity $u_\mu(t,r)$ should be taken, for details see [23] . (We ignore changes in the equation of state at $T > T_c$.)

Note first, that while the absolute sizes and multiplicities in central AA are quite different

from pA and pp bins discussed, in the dimensionless variables those are not so far away. Notably the pA freezeout appears "later" than for AA, and pp later still. (Of course, the order is opposite in the absolute fm units.) Thus illustrates the case we made with the thought experiment 2: smaller systems gets more and more "explosive", because in the right units CD path is longer than AD.

The transverse collective velocity on the freeze out curves is read off (8). We would not give here a plot but just mention that transverse rapidity rise about linearly from the fireball center to the the maximal values reached at the "corner" of the freeze-out curves. For three cases considered those are

$$v_\perp^{max}[AA, pA, pp] = [0.69, 0.83, 0.95] \qquad (16)$$

These values are of course for qualitative purposes only, to demonstrate the point in the most simple way. We will discuss recent CMS data and realistic freezeout surfaces corresponding to them at the end of the paper.

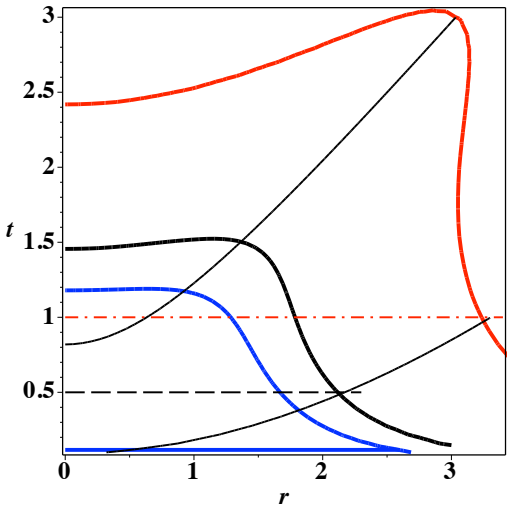

FIG. 2: (color online) The three horizontal lines correspond to the initial time: from bottom up AA (blue solid), pA (dash black) and pp (red dash-dot). The corresponding three curves with the same color are the lines at which the temperature reaches the same freeze-out value, set to be $T_f = 150\,MeV$. The two thin solid lines correspond to the values of the variable $\rho = -2.2$ (lower) and -0.2 (upper). Those values are used as initial and final values in the evolution of higher harmonics.

B. The Navier-Stokes corrections

We continue to discuss the radial flow adding the first viscosity effect. The equation for the reduced temperature $\hat{T} = \hat{\epsilon}^{1/4}$ using the combination of variables

$$g = \frac{1 - t^2 + r^2}{2t} \qquad (17)$$

becomes an ordinary differential equation

$$3(1+g^2)^{3/2}\frac{d\hat{T}}{dg} + 2g\sqrt{1+g^2}\hat{T} + g^2 H_0 = 0 \qquad (18)$$

This equation is easily solvable analytically in terns of certain hypergeometric functions or numerically. Note that the last term contains viscous parameter

$$H_0 = \frac{\eta}{\epsilon^{3/4}} = \frac{\eta}{s}\frac{4}{3} f_*^{1/4} \qquad (19)$$

For $\eta/s = 0.134$ one finds $H_0 = 0.33$ we will use as representative number.

The question is how important is the viscous term. While H_0 is just a constant, its role depends on the magnitude of the initial temperature $\hat{T}_0$ or total entropy. For AA collisions we find that its role is truly negligible, as the curves hardly are separated by the line width. (This is, of course, well known from all studies in the literature.) For the pA and pp cases as modeled above one can see a difference between ideal and viscous solutions , shown in Figs. 3 through the temperature dependence $T = \hat{T}/t$ at certain positions. The viscous effect is maximal at early times, while the viscous and ideal curves meet near freezeout. As expected, the viscous effects are more noticeable at the fireball edge, compare the $r = 1$ and the $r = 3$ plots. The main conclusion of this section is that small viscosity of the sQGP provides only modest corrections to the radial flow, even for the pA and pp cases.

Another sourse of viscous corrections comes from modifications of the particle distributions induced by gradients of the flow. Those should be proportional to tensor of flow derivatives at

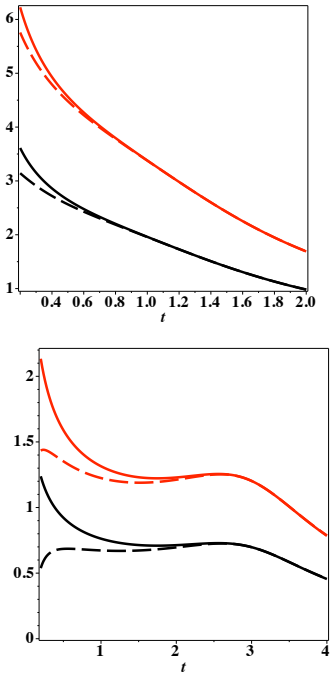

FIG. 3: (color online) The temperature versus dimensionless time t, for ideal hydrodynamics (solid) and viscous hydrodynamics with $\eta/s = 0.132$ (dashed) lines. The upper pair of (red) curves are for pp, the lower (black) ones for pA collisions. The upper plot is for $r = 1$, the lower plot for $r = 3$.

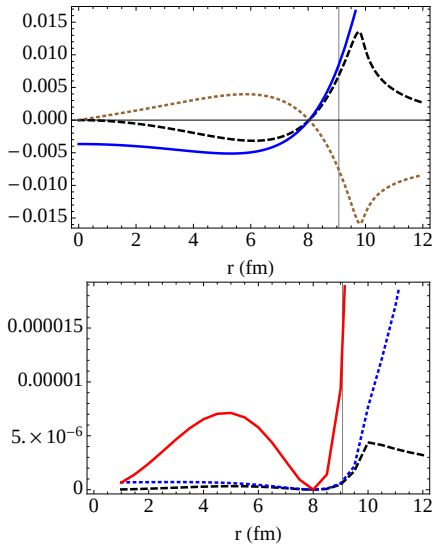

FIG. 4: (color online) Radial dependence of the first order viscous term (a) and the second order one (b) for central AA collisions. In (a) the black dashed,blue solid, and brown dotted lines show 00,11,01 components of $\sigma_{\mu\nu}$, respectively. In (b) we show 00,11,22 components of (23) by black dashed, blue dotted and red solid lines.

the freezeout surface

$$\delta f(x,p) \sim f(x,p) p^\mu p^\nu u_{\mu;\nu} \qquad (20)$$

where semicolon as usual stands for covariant derivative. The coefficient is to be determined from the fact that this correction is the one inducing the viscosity part of the stress tensor. Looking at the space-time dependence of the (symmetrized) tensor of flow covariant derivatives

$$\sigma_{\mu\nu} = u_{<\mu;\nu>} \qquad (21)$$

we found rather curious behavior produced by Gubser's flow. In Fig.4 we display several components of this tensor, and one can see that some of them change sign and magnitude at $r \approx 10\, fm$, which is on the r.h.s. or space like part of the freezeout surface in AA collisions. (The "corner" in this case is at $r \approx 9.1\, fm$.) We think that this behavior is in fact an artifact of the Gubser solution caused by slow (power-like) decrease of the density at large distance. This tails of the matter distribution serve in fact as an"atmosphere" around the fireball, in which some fraction of expanding matter get accelerated inwards. We checked that such behavior is not observed for exponentially decaying tails, as is the case for real nuclei. Our conclusion then is that one should not use Gubser solution outside of the fireball "rim", in our case for $r > 9.1\, fm$. Fortunately, with realistic nuclear shapes that part of the surface contribute only very small – few percents – contribution to particle spectra and can therefore be neglected.

Let us now start the discussion of the second and higher order gradients. In general, those can be treated phenomenologically: one can write down a complete set of all possible forms for the stress tensor of the given order, with some coefficients to be determined empirically. The corresponding contribution to the

stress tensor looks like

$$\pi^{\mu\nu} = \sum_n c_n P_n^{\mu\nu}(T, u^\alpha) \sim \sum_n c_n \left(\frac{1}{TR}\right)^n \tag{22}$$

with some coefficients c_n and certain kinematical structures with i derivatives $P_n^{\mu\nu}$. Their order of magnitude is given by the pertinent powers of the hydro parameter $1/TR$, or multiplcity. Unfortunately, even for the second gradients there are way too many terms for that to be a practical program .

For conformal fluids the number of the second order terms is more manageable and using the AdS/CFT one can obtain the value of the coefficients (for review see [16]). Using such as a guide, one can estimate the magnitude of the terms neglected in the Navier-Stokes approximation. Furthermore, for Gubser flow we find that the rotational (antisymmetric) combination of the covariant derivatives $\omega_{\alpha,\beta} = u_{[\alpha;\beta]} = 0$, which eliminates two more terms. The term which is the easiest to estimate is the symmetrized convolution of two first order term

$$\pi^{(2)}_{\mu\nu} = -\frac{\lambda_1}{2}\sigma_{<\mu\lambda}\sigma^{\lambda}_{\nu>} \tag{23}$$

where angular bracket stands for symmetrization of $\mu\nu$. The AdS/CFT value for the coefficient is $\lambda_1 = \eta/(2\pi T)$.

Radial dependence of this term at the freeze-out surface for AA collision is shown in Fig.4 (b). It is reasonably small and constant, except strong growth "beyond the rim" of the fireball. As we already noted above, this is the artifact of the Gubser solution, which should be ignored.

C. The radial expansion and the Israel-Stuart second-order hydrodynamics

Using the lowest order hydrodynamics equations one can trade the spatial derivatives by the time ones, and subsequently promote the "static" gradient tensor $\sigma^{\mu\nu}$ to "dynamical" stress $\pi^{\mu\nu}$, with its own equaltion of motion. One may wander how these equations behave in the Gubser setting.

Since the first version of this paper was posted, this was done in [12], which we follow in this section. The main purpose of this paper has been methodical, to check their previously developed MUSIC hydro solver against the analytically solvable examples. (The solutions discussed were not intended to correspond to any particular physical settings.)

The IS equations to be solved have in this case the form

$$\frac{\hat{T}'(\rho)}{\hat{T}(\rho)} + \frac{2}{3}tanh(\rho) = \frac{1}{3}\pi(\rho)tanh(\rho) \tag{24}$$

$$c\frac{\eta}{s}[\pi'(\rho)+\frac{4}{3}\pi(\rho)^2 tanh(\rho)]+\pi(\rho)\hat{T}(\rho) = \frac{4}{3}\frac{\eta}{s}tanh(\rho) \tag{25}$$

where a prime denotes the derivative over the "time" ρ, and

$$\hat{T} = T\tau, \quad \pi(\rho) = \hat{\pi}^{\xi}_{\xi}\frac{1}{\hat{T}\hat{s}} \tag{26}$$

Note that at $\rho \to \pm\infty$ the dimensionless temperature $\hat{T}$ vanishes as certain negative power of $cosh\rho$, and therefore the second eqn decouples from the first. Furthermore, putting to zero the derivative, one find constant fixed point solution $\pi = 1/\sqrt{c}$, to which any solution should tend in the $\rho \to \pm\infty$ limit. This feature is very unusual, in variance with Navier-Stokes and generic dissipative equations, which only regulate solutions at positive time infinity, generating singular or indefinitely growing solutions toward the past $\rho \to -\infty$. In this sense, there exists clear advantage of the IS equations over the NS ones: but we don't think this improvement reflects actual physics.

The negative of the Israel-Stuart version of hydrodynamics, is that selecting the initial conditions for $\pi(\rho)$ is a nontrivial task. In principle, some theory of pre-equilibrium conditions – e.g. the AdS/CFT or color glass condensate (CGC) model – should provide it. For lack of knowledge about the initial value of the anisotropic part of the pressure tensor $\pi^{\mu\nu}$ practitioners often select $\pi(\tau_i) = 0$ at the initiation time, and then carry it on from the equation, till freezeout. In Fig.5 such a solution to Israel-Stuart equations given above is shown by the black solid lines. This solution is indeed more than satisfactory, in the sense that the temperature is very close to the ideal case (red dotted line), and π remains small.

This however is opposite to general expectations for the real QCD setting, in which the

coupling constant runs from small to large as a function of time. Because of that, the $\eta/s, c$ are not in fact constant but run, toward the most ideal fluid reached near T_c, at the end of the QGP era. Therefore one expects the non-equilibrium effects – in particular described by π – to monotonously decrease from the initial to the final state, as close to equilibrium as possible. We therefore suggest another possible solution, with $\pi(\rho)$ set to be zero at the end of the expansion, at the freezeout. This solution is shown in Fig.5 by the blue dashed line: it indeed shows a monotonous decrease of $\pi(\rho)$ in the range of interest, $\rho = -2..0$. While this scenario it is not as nice as the previous one – the anisotropic pressure is not small at the initial time $\pi(-2) \sim 1$ and in the temperature deviations from the ideal solution are well seen – perhaps it is closer to reality.

In summary, while IS approach has advantages such as regular behavior of the solutions at both time infinities, in practice it allows wide range of solutions in between, depending on the required initial conditions for the viscous tensor. There is no real argument explaining why this version can be better than the first order NS in cases when viscous corrections get noticeable, as there is no estimate of the terms neglected.

D. Higher gradients and Lublinsky-Shuryak re-summation

The Navier-Stokes and Israel-Stuart approximations used so far only includes the first and the second order terms in the gradient expansion. What about high orders?

The expansion coefficients may be obtained from AdS/CFT, an indispensable tool. For small (linearized) perturbations – sounds – the correlators of the two stress tensors was calculated to higher orders in frequency and wave vector ω, k, extending the original viscosity prediction $\eta/s = 1/4\pi$ of Son et al to about a dozen further coefficients.

Can one re-sum the higher gradient terms? While hydrodynamics is more than two centuries old, it seems that the first attempt of the kind has been suggested by Lublinsky and Shuryak (LS) [20]. An approximate PADE-like re-summation of the higher order terms results

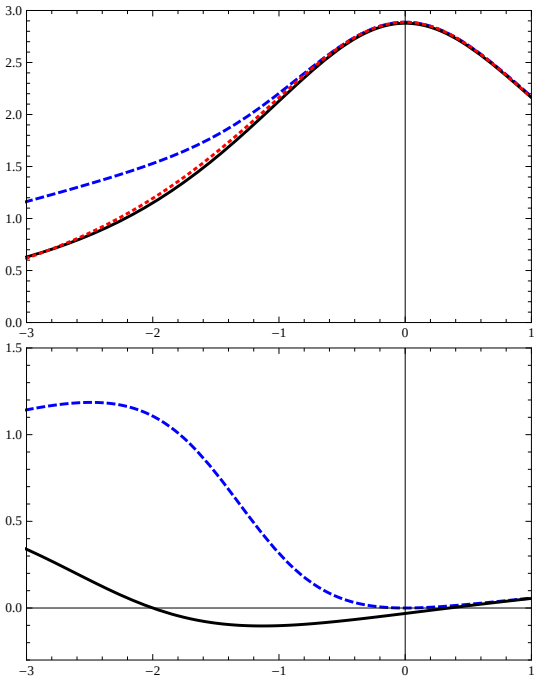

FIG. 5: (color online) (a) The dimensionless conformal temperature $\hat{T}$ and (b) the dimensionless conformal stress π as a function of "time" ρ. The parameters correspond to $q = 1\, fm^{-1}, \eta/s = .2, c = 5$ and multiplicity corresponding to the highest multiplicity bin of pA in CMS experiment. The red dotted line in (a) is the ideal hydro Gubser solution $\hat{T}_0/cosh^{2/3}\rho$. In both plots the blue dashed lines are for a "realistic" solution with $\pi(0) = 0$ near freezeout, while the black solid lines are for "nice" solution with zero anisotropic stress at the initiation time, $\pi(-2) = 0$.

from the alternating signs of the series and coefficients of the order 1, which calls for approximate re-summation *a la* geometrical series[31]

$$1 - x + x^2 + \ldots \to \frac{1}{1+x} \tag{27}$$

which keeps the quantity positive and regular even for $x > 1$. The suggested recipe is to substitute the Navier-Stokes viscosity constant by an effective one, which is in frequency-momentum dependent and reads

$$\eta_{LS2}(\omega, k) = \frac{\eta_{NS}}{1 - \eta_{2,0}k^2/(2\pi T)^2 - i\omega\eta_{0,1}/(2\pi T)} \tag{28}$$

while (28) involves only two dimensionless coefficients, whose values for AdS/CFT are

$$\eta_{2,0} = -\frac{1}{2}\ \eta_{0,1} = 2 - \ln 2 = 1.30 \qquad (29)$$

it actually approximately reproduces about a dozen of known terms. Note that re-summation into the denominator suggests a *reduction* of the viscous effect as gradient grows. It may look counterintuitive: note however that viscosity is a coefficient of a term in hydro equations with at list second order of k: so this reduction only makes such terms finite, not zero.

Recently one of us has studied the "strong shock wave" problem [25] in the AdS/CFT setting, solved from the first principles (Einstein equations) and comparing to the LS resummation. While this problem is far from sound and is a generic "hydro-at-its-edge" type, with large gradients without any small parameters, deviations between the NS and the exact (variational) solution of the corresponding Einstein equations were found to be on the level of few percents only. Studies of time-dependent collisions in bulk AdS/CFT have found that the first-principle solution approaches the NS solution early on and quite accurately, at the time when the higher gradients by themselves are not small, see e.g. [26].

Let us now check how does it work in the case of Gubser solution. Changing k^2, ω into derivatives

$$\begin{aligned} -k^2/q^2 \ &\to\ (\frac{\partial}{\partial r})^2 + \frac{1}{r}\frac{\partial}{\partial r} \\ i\omega/q \ &\to\ \frac{\partial}{\partial t} \end{aligned} \qquad (30)$$

makes the re-summed factor (with the denominator) an integral operator, which can be used not only for plane waves of the sound but for any function of the coordinates $f(t,r)$. The inverse "LS operator" acting on a function f is defined as

$$\begin{aligned} \mathbf{O}^{-1}_{LS}(f) = \quad & 1 + \frac{q^2}{2(2\pi T)^2}\left(\frac{\partial^2 f}{\partial r^2} + \frac{1}{r}\frac{\partial f}{\partial r}\right)\frac{1}{f} \\ & + (2-\ln 2)\,\frac{q}{2\pi T}\frac{\partial f}{\partial t}\frac{1}{f} \end{aligned} \qquad (31)$$

Schematically the resummed hydro equations look as

$$(Euler) = \eta \mathbf{O}_{LS}(Navier - Stokes) \qquad (32)$$

where $\mathbf{O}_{LS}$ is an integral operator. However, one can act with its inverse on the hydrodynamical equation as a whole, acting on the Euler part but canceling it in the viscous term

$$\mathbf{O}^{-1}_{LS}(Euler) = \eta(Navier - Stokes) \qquad (33)$$

These are the equations of the LS hydrodynamics. Obviously they have two extra derivatives and thus need more initial conditions for solution.

Instead of solving these equations, we will simply check the magnitude of the corrections appearing in the l.h.s due to the action by the LS differential operator on the (ideal Gubser) solution used as a zeroth-order starting point. As one can see, large systems have a small $q/T \sim 1/RT$ parameter and so these corrections are *parametrically* small. The issue is what happens "on the hydro edge", when the corrections have no formal small parameter.

In Fig.6 we show the (inverse) action of (31) on the zeroth other temperature profile of the Gubser flow as a function of r. We have used the freeze-out temperature $T_f = 150\,MeV$ and the indicated respective freeze-out times for pp, pA and AA. The higher gradient corrections for AA and pA are inside the few percent range from 1, while in the pp case the correction is larger, yet still in the 15 percent range. We thus conclude, that if the LS resummation represents the role of the higher gradients, the overall corrections remain manageable, although it does grow from AA to pA to pp cases.

III. HIGHER ANGULAR HARMONICS

A. Acoustic damping

There is a qualitative difference between the radial flow we had discussed so far, and higher angular harmonics. While the former monotonously grows with time, driven by sign-constant pressure gradient, the latter are a (damped) oscillators. The signal observed depend on the viscous damping factor as well as on the particular phase in which the oscillator finds itself at the freezeout time. We will discuss those effects subsequently.

The effects of viscosity damps the higher angular flow moments stronger. The so called

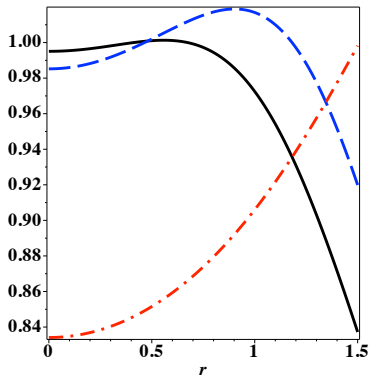

FIG. 6: (color online) The action of the LS operator O_{LS} (31) on the zeroth order (non-viscous) temperature profile, the first term of (40). The three lines correspond to AA (black) solid, pA (blue) dashed and pp (red) dash-dot.

"acoustic damping" formula was suggested by Staig and Shuryak [21] . Wave amplitude reaction is given by

$$P_k = \frac{\delta T_{\mu\nu}(t,k)}{\delta T_{\mu\nu}(0,k)} = \exp\left(-\frac{2}{3}\frac{\eta}{s}\frac{k^2 t}{T}\right) \qquad (34)$$

Since the scaling of the freeze out time is linear in R or $t_f \sim R$, and the wave vector k corresponds to the fireball circumference which is m times the wavelength

$$2\pi R = m\frac{2\pi}{k} \qquad (35)$$

the expression (34) yields

$$\frac{v_m}{\epsilon_m} \sim \exp\left[-m^2\frac{4}{3}\left(\frac{\eta}{s}\right)\left(\frac{1}{TR}\right)\right] \qquad (36)$$

Note that the exponent contains the product of two small factors, η/s and $1/TR$, as discussed in the introduction. Note further that the harmonics number is squared. For central PbPb LHC collisions with

$$\frac{1}{TR} = \mathcal{O}(1/10) \qquad (37)$$

its product of η/s is $O(10^{-2})$. So one can immediately see from this expression why harmonics up to $m = O(10)$ can be observed.

Proceeding to snapper systems in the spirit of our thought experiment 0, by keeping a similar initial temperature $T_i \sim 400\,MeV \sim 1/(0.5\,fm)$ but a smaller size R, results in a macro-to-micro parameter that is no longer small, or $1/TR \sim 0.5, 1$, respectively. For a usual liquid/gas, with $\eta/s > 1$, there would not be any small parameter left and one would have to conclude that hydrodynamics is inapplicable for such a small system. However, since the quark-gluon plasma is an exceptionally good liquid with a very small η/s, one can still observe harmonics up to $m = O(\sqrt{10}) \sim 3$. However, if $TR = const$, along the line of the thought experiment 1, there is no difference in the damping.

Extensive comparison of this expression with the AA data, from central to peripheral, has been recently done in Ref. [22] . Both issues – the m^2 and $1/R$ dependences of the $log(v_m/\epsilon_m)$ – are very well reproduced. It works all the way to rather peripheral AA collisions with $R \sim 1\,fm$ and multiplicities comparable to those in the highest pA binds. Thus the acoustic damping provides solid hydro-based systematics of the harmonic strength, to which new pA and pp data should be compared.

B. Angular harmonics of Gubser flow

Unfortunately, the acoustic damping formula does not include the oscillatory prefactors. (As emphasized in Ref. [23], those should lead to secondary peaks in power spectrum of fluctuations at high m similar to those in cosmological perturbations. Those are however not yet observed.)

Since we are actually interested in not so large $m = 2, 3$, we return to Gubser's flow and consider its angular perturbations. Those has been developed in [19, 23]. In the former paper Gubser and Yarom re-derived the radial solution by going into the co-moving frame via a coordinate transformation from the τ, r to a new set ρ, θ given by:

$$\sinh\rho = -\frac{1-\tau^2+r^2}{2\tau} \qquad (38)$$

$$\tan\theta = \frac{2r}{1+\tau^2-r^2} \qquad (39)$$

In the new coordinates the rescaled metric reads:

$$d\hat{s}^2 \;=\; -d\rho^2 + \cosh^2\rho\left(d\theta^2 + \sin^2\theta d\phi^2\right) + d\eta^2$$

and we will use ρ as the "new time" coordinate and θ as a new "space" coordinate. In the new coordinates the fluid is at rest, so the velocity field has only nonzero u_ρ. The temperature is now dependent only on the new time ρ. For nonzero viscosity the solution is

$$\hat{T} = \frac{\hat{T}_0}{(\cosh\rho)^{2/3}} + \frac{H_0\sinh^3\rho}{9(\cosh\rho)^{2/3}} \times {}_2F_1\left(\frac{3}{2},\frac{7}{6};\frac{5}{2},-\sinh^2\rho\right) \qquad (40)$$

with $\hat{T} = \tau f_*^{1/4} T$ and $f_* = \epsilon/T^4 = 11$ as in [18].

Small perturbations to Gubsers flow obey linearized equations which have also been derived in [19]. We start with the zero viscosity case, so that the background temperature (now to be called T_0) will be given by just the first term in (40). The perturbations over the previous solution are defined by

$$\hat{T} \;=\; \hat{T}_0(1+\delta) \qquad (41)$$

$$u_\mu \;=\; u_{0\,\mu} + u_{1\mu} \qquad (42)$$

with

$$\hat{u}_{0\,\mu} \;=\; (-1,0,0,0) \qquad (43)$$

$$\hat{u}_{1\mu} \;=\; (0,u_\theta(\rho,\theta,\phi),u_\phi(\rho,\theta,\phi),0) \qquad (44)$$

$$\delta \;=\; \delta(\rho,\theta,\phi) \qquad (45)$$

The exact solution can be found by using the separation of variables $\delta(\rho,\theta,\phi) = R(\rho)\Theta(\theta)\Phi(\theta)$. In the non-viscous case, that we are now discussing, each of the three equations

$$R(\rho) + \frac{4}{3}\tanh\rho R(\rho) + \frac{\lambda}{3\cosh^2\rho}R(\rho) = 0$$

$$\Theta(\theta) + \frac{1}{\tan\theta}\Theta(\theta) + \left(\lambda - \frac{m^2}{\sin^2\theta}\right)\Theta(\theta) = 0$$

$$\Phi(\phi) + m^2\Phi(\phi) = 0 \qquad (46)$$

are analytically solvable, with the results discussed in [23]. The parts of the solution depending on θ and ϕ can be combined in order to form spherical harmonics $Y_{lm}(\theta,\phi)$, such that $\delta(\rho,\theta,\phi) \propto R_l(\rho)Y_{lm}(\theta,\phi)$.

The basic equations for the ρ-dependent part of the perturbation, now with viscosity terms, can be written as a system of coupled first-order equations [19]. We are assuming rapidity independence, thus the system of equations (107),(108) and (109), from the referred paper, becomes two coupled equations, for (the ρ-dependent part of) the temperature and velocity perturbations

$$\frac{d\vec{w}}{d\rho} = -\Gamma\vec{w}\;, \quad \vec{w} \;=\; \begin{pmatrix}\delta_v\\ v_v\end{pmatrix} \qquad (47)$$

where the index v stands for viscous and the matrix components are,

$$\Gamma_{11} = \frac{H_0\tanh^2\rho}{3\hat{T}_b}$$

$$\Gamma_{12} = \frac{l(l+1)}{3\hat{T}_b\cosh^2\rho}\left(H_0\tanh\rho - \hat{T}_b\right)$$

$$\Gamma_{21} = \frac{2H_0\tanh\rho}{H_0\tanh\rho - 2\hat{T}_b} + 1$$

$$\Gamma_{22} = (8\hat{T}_b^2\tanh\rho + H_0\hat{T}_b\left(\frac{-4(3l(l+1)-10))}{\cosh^2\rho} - 16\right) + 6H_0^2\tanh^3\rho)/(6\hat{T}_b\left(H_0\tanh\rho - 2\hat{T}_b\right)) \qquad (48)$$

Before we display the solutions, we need to translate our space-time plot into the $\rho-\theta$ coordinates. The initiation surface $t = t_i$ are *not* the $\rho = const$ surfaces. The freezeout ones also do not correspond to fixed ρ because the temperature is $T = \hat{T}(\rho)/t(\rho,\theta)$. So, in both cases one has to decide which points on the initiation and final surfaces are most important. The thin solid lines in Fig.2 approximately represent the initial ρ_i and the final ρ_f values for all three systems. Therefore, we will solve the equations between those two surfaces.

In Fig.7 we show the solution of the ρ evolution of the two variables, the temperature perturbation and velocity $\delta_l(\rho), v_l(\rho)$. As one can see, all of them start at $\rho_0 = -2$ from the same $\delta_l = 1$ value. While the elliptic one $l = 2$ (black solid curves) changes more slowly, higher harmonics oscillate more. We return to its discussion in section IV B

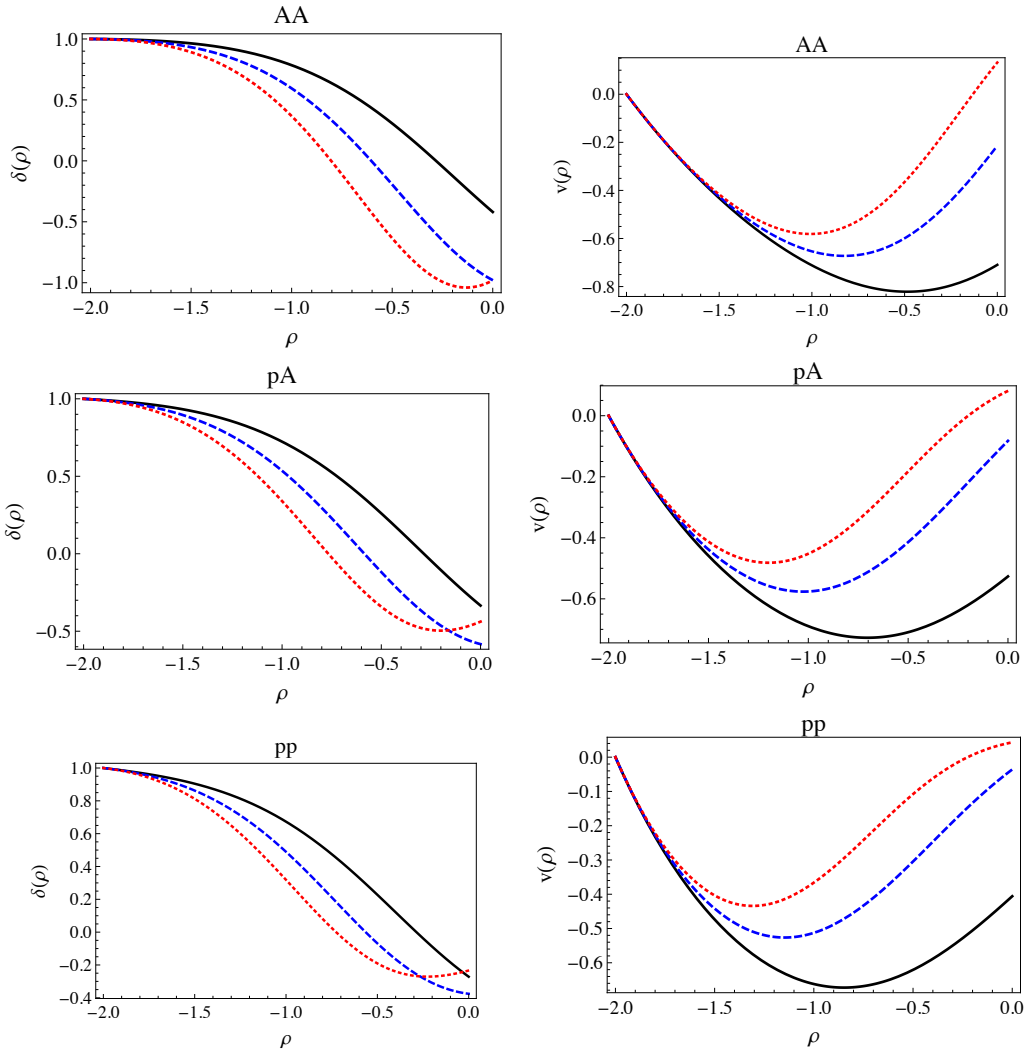

FIG. 7: (color online) The dimensional less temperature perturbation $\delta_l(\rho)$ and velocity $v_l(\rho)$, for $l = 2, 3, 4$ shown by (black) solid, (blue) dashed and (red) dotted curves, respectively. Three sets of calculations corresponds to AA, pA and pp collisions.

IV. PHENOMENOLOGY

A. The radial flow in spectra of identified secondaries

The main idea behind experimental signatures of the radial flow has been used in [3], it is based on the fact that collective flow manifests itself differently for secondaries of different mass. The exponential thermal spectra of the near-massless pion are simply blue-shifted by a factor, the exponent of the transverse flow rapidity $T' = Te^{\kappa}$. However spectra of massive particles – such as kaons, protons etc – are modified in a more complex way. Instead of discussing the shape of the spectra, let us focus on their high-momentum behavior and the so called $m_\perp$ slopes: the particle spectra are fit-

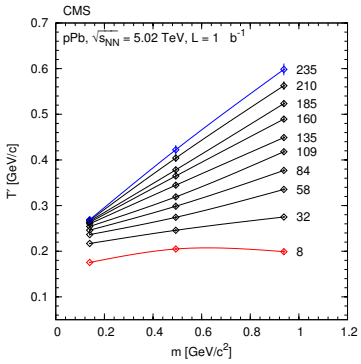

FIG. 8: (color online) The slopes of the $m_\perp$ distribution T' (GeV) as a function of the particle mass, from [13]. The numbers on the right are track multiplicity.

ted to the exponential form (above certain p_t)

$$\frac{dN}{dydp_\perp^2} = \frac{dN}{dydm_\perp^2} \sim exp(-\frac{m_\perp}{T'}) \qquad (49)$$

in the transverse mass variable $m_\perp = \sqrt{m^2+p_\perp^2}$, typically above certain value of the $m_\perp$ (see examples below). It has been found in [3] using the min.bias ISR pp data that the so called "$m_\perp$ scaling" holds – the slopes T' are *the same* for π, K, p independent on their mass M. This scaling (coming from the string fragmentation mechanism) implies that there was *no* evidence for collective expansion in min.bias. pp collisions at the ISR energies.

Recent CMS pA data [13] significantly increased the range of multiplicities, and now contain spectra of identified particles. As seen in the shown in Fig.8, for small multiplicity bins (marked by 8 and 32 at the bottom) the same $m_\perp$ scaling holds, 34 years later and at beam energies hundreds of times higher. However for larger multiplicity bins the slopes grow with the particle mass linearly. Qualitatively similar behavior has been previously seen in AGS/SPS/RHIC and LHC AA data, and is widely recognized as *the signature* of the radial flow. Furthermore, six months after the first version of this paper [1] made its main prediction – that not only the radial flow in pA and pp will be observed, but that its magnitude will even be *larger* than in central AA collisions – is confirmed. The highest multiplicity pA do have slopes exceeding even those in central PbPb LHC collisions, the previous record-holding on the radial flow.

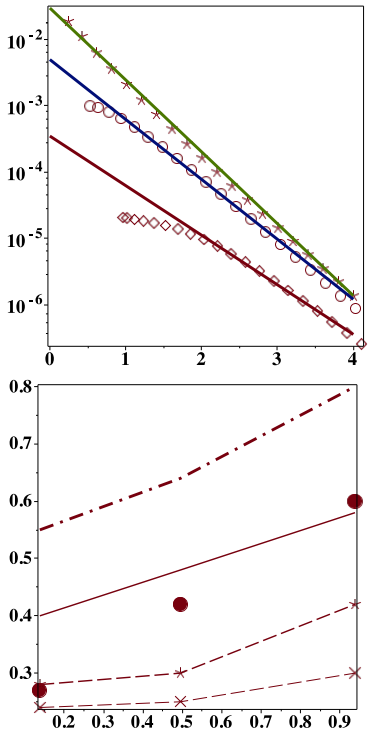

FIG. 9: (color online) (a) A sample of spectra calculated for π, K, p, top-to-bottom, versus $m_\perp$ (GeV), together with fitted exponents. (b) Comparison of the experimental slopes $T'(m)$ vests the particle mass m (GeV). The solid circles are from the highest multiplicity bin data of fig.(a), compared to those of the theoretical models. The solid and dash-dotted lines are our calculations for freezeout temperatures $T_f = 0.17, 0.12\, GeV$. Asterisks/dashed line are for Epos LHC, diagonal crosses /dashed line are for AMTP models.

In Fig.9(a) we show samples $m_\perp$ spectra calculated from Gubser radial flow. As for any axially symmetric case, one can perform the integrals over the spatial rapidity and azimuthal angle analytically, both producing Bessel func-

tions,

$$\frac{dN}{dydp_\perp^2} = \frac{g_{stat}}{2\pi^2}\int dr\tau(r)r \quad (50)$$
$$[m_\perp K_1(\frac{m_\perp cosh(\kappa)}{T_f})I_0(\frac{p_\perp sinh(\kappa)}{T_f})$$
$$-p_\perp \frac{d\tau}{dr}K_0(\frac{m_\perp cosh(\kappa)}{T_f})I_1(\frac{p_\perp sinh(\kappa)}{T_f})]$$

In the remaining radial Cooper-Fry integral over the freezeout surface one should substitute proper time $\tau(r)$ and its derivative, as well as transverse rapidity $\kappa(\tau(r), r)$, defined via $\tanh(\kappa) = v_\perp$. The spectra are fitted to exponential form at large $m_\perp$ (see Fig.9(a)) and finally in Fig.9(b) we compare the slopes T' observed by the CMS (in the highest multiplicity bin) to theoretical results.

We start doing it by comparing to other models. We do not include the parton cascade models Hijing, as it has no flow by design and obviously fails in such a comparison. The (latest version of the) hydrodynamical model "Epos LHC" [14] predicts spectra with slopes shown by asterisks: as evident from Fig(b) it misses the slope by a lot, for the protons by about factor 2. Even further from the data are the slopes calculated from the AMPT model [15] (diagonal crosses and dashed line).

Upper two lines in Fig.9(b) show our results, corresponding to two selected values of T_f, .12 and .17 GeV. The former is in the ballpark of the kinetic freezeout used for AA data: but as the figure (b) shows it overpredicts the radial flow for the pA case. The second value corresponds to the QCD critical temperature T_c: it is kind of the upper limit for T_f since it is hard to imagine freezeout in the QGP phase. As seen from the figure, such value produces reasonable amount for the collective radial flow as observed by the CMS. The same level of agreement holds not only in the highest multiplicity bin, but for most of them. We thus conclude that in pA the chemical and kinetic freezeout coincide.

Apart from the effective $m_\perp$ slopes T' for each multiplicity bin and particle type, the paper [13] also gives the mean transverse momenta. Like slopes, they also display that radial flow in few highest multiplicity pA do exceed that in central AA. Those data also agree reasonably well with our calculation.

(The reader may wander why we don't compare the spectra themselves. Unfortunately we cannot do it now, neither in normalization more in shape because of significant "feeddown" from multiple resonance decays, strongly distorting the small-p_t region. Event generators like HIJING and AMPT use "afterburner" hadron cascade codes for that.)

B. Higher harmonics

The repeated motive of this paper is that the smaller systems should have stronger radial flow, as they evolve "longer" (in proper units, not absolute ones) and the pressure gradient driving them never disappears. Higher harmonics are not driven permanently but are instead oscillating, plus damped by the viscosity. Since the only harmonics in the pA and pp observed so far are the elliptic $m = 2$ and triangular $m = 3$ ones, and their origins are quite different, we will discuss them subsequently, starting from qualitative expectations and then returning to hydro calculations.

Elliptic deformation ϵ_2^{AA} of the peripheral AA collisions is quite large, significantly larger than than those of the very central pA ϵ_2^{pA} of comparable multiplicity. However if those are evaluated – e.g. in the Glauber model – and divided out in the ratio v_2/ϵ_2, the result should be about the same in both cases for the same multiplicity in both sets. This is e.g. seen from the acoustic damping expression (36): the same value of the multiplcity/entropy implies the same TR and thus damping.

Specially interesting case is dAu collisions, as in this case there are two collision centers and ϵ_2 is factor 2 enhanced [11], and v_2 is also a factor 2 higher [9]

The m=3 flow originates from fluctuations, not from a particular average shape. Therefore[32] , assuming we compare the same number of wounded nucleons and multiplicity in central pA and peripheral AA, we expect similar ϵ_3 in both cases. Indeed, the magnitude of all $m > 2$ deformations is $\epsilon_{m>2} \sim 1/\sqrt{N}$ where N is the number of "fluctuating clusters" – wounded nucleons. Thus we expect v_3 for both cases be *the same*, even without the need to renormalize it by ϵ_3. This predictions

is indeed fulfilled in the LHC data.

Now we return to hydro results, discussed in section III B. As one can see from Fig.7 the time from initial $\rho \sim -2$ till freezeout $\rho \sim 0$ is between a quarter and a half of the period of the oscillations. So the energy associated with the initial spatial deformation is transferred into kinetic energy of the flow, and start to come back when the explosion ends. The amplitude of the velocity at the r.h.s. of the plot is the largest for the m=2, and is smaller for m=3,4. Smaller system do evolve a bit "longer" which put their velocity amplitudes closer to zero.

Note that all of those start from the same deformation ϵ_m, so what one reads from this plot is actually proportional to v_m/ϵ_m. In order to get absolutely normalized v_m/ϵ_m one has to do integration over the the Cooper-Fry freezeout, as done in the previous section for radial flow. Since the latter includes rather lengthy calculations (see [23] for details) we will not do it at this stage.

Assuming that the integrals produce the same factors for all cases, we just read off the ratios of v_m/ϵ_m from Fig.7 values of the flow at $\rho \sim 0$. Since measurements are for two-particle correlation functions, we compare the *squares* of the flow harmonics

$$\begin{aligned}&(\frac{v_2^{AA}}{\epsilon_2^{AA}})^2 : (\frac{v_2^{pA}}{\epsilon_2^{pA}})^2 : (\frac{v_2^{pp})}{\epsilon_2^{pp}})^2 \\ &= 0.5 : 0.3 : 0.16 \end{aligned} \tag{51}$$

(This is not inconsistent with constancy of the v_2/ϵ_2 proposed above, since in the calculations we do not compare three points on the same adiabatic or $RT = const.$)

The CMS data do show that the pp has smaller v_2 as compared to pA data, the ratio is about a factor of 1/4 (see Fig.3 of [6]) rather than 1/2 which the hydro solution provides. Perhaps it is because the pp collisions create a somewhat more spherical fireball, with $\epsilon_2^{pp} < \epsilon_2^{pA}$, in spite of having a smaller size. We will return to this issue at the end of the paper.

Let us now compare in a similar manner the ratio of the $m = 3$ to $m = 2$ harmonics

$$\begin{aligned}\left(\frac{v_3^{AA}}{v_2^{AA}}\right)^2 &\approx 0.12 \left(\frac{\epsilon_3^{AA}}{\epsilon_2^{AA}}\right)^2 \\ \left(\frac{v_3^{pA}}{v_2^{pA}}\right)^2 &\approx 0.09 \left(\frac{\epsilon_3^{pA}}{\epsilon_2^{pA}}\right)^2 \\ \left(\frac{v_3^{pp}}{v_2^{pp}}\right)^2 &\approx 0.02 \left(\frac{\epsilon_3^{pp}}{\epsilon_2^{pp}}\right)^2 \end{aligned} \tag{52}$$

Assuming $\epsilon_3/\epsilon_2 \sim 1$ one finds that in pA we predict $v_3/v_2 \approx 1/3$, which agrees nicely with the ALICE data [7]. For pp we have $v_3/v_2 \approx 1/7$ which is probably too small to be seen.

C. Comment of higher gradients at freezeout

The effect of flow gradients affect spectra at freezeout. As emphasized by Teaney [27], the equilibrium distribution function $f_0(x,p)$ should be complemented by the non equilibrium corrections proportional to flow gradients

$$\begin{aligned}f(x,p) = \quad & f_0(x,p) + \delta f(x,p) p^\mu p^\nu \partial_\mu u_\nu \\ & + (\text{higher gradients}) \end{aligned} \tag{53}$$

Furthermore [27] , the Lorentz covariance forces any extra gradient to carry another power of the particle momentum. As a result, the expansion parameter of the n-th term is of the order

$$\frac{\delta f}{f} \sim \frac{\eta}{s} \left(\frac{p}{T}\frac{1}{TR}\right)^n \tag{54}$$

If one moves to large $p_\perp/T = \mathcal{O}(10)$, compensating small factor $1/TR$, the expansion in gradients (and thus hydrodynamics) breaks down. Indeed, the radial and harmonics of the flow agree with hydro up to transverse momenta of the order of $p_t \approx 3\,\text{GeV}$, or $p_t/T_f < 20$.

In some applications people had calculated $f + \delta f$ and get negative spectra at large p_t from viscous corrections, which is of course meaningless. Needless to say, it resemble the first terms $(1-x)$ in expansion (27), which gets negative for $x > 1$. Our suggestion, along the line of LS re-summation, is to use instead

$$f = \frac{f_0}{1 + \delta f/f_0} \tag{55}$$

form which is sign-definite and approximately reproduce the higher order terms as well.

V. SUMMARY AND DISCUSSION

High multiplicity pp and pA collisions are very interesting systems to study, as they are expected to display the transition from a "micro" to "macro" dynamical regimes, treated theoretically by quite different means. In this paper we tried to explain how this transition works using the language of the macroscopic theory, the viscous hydrodynamics.

As we emphasized in the Introduction, the applicability of hydrodynamics to high energy collisions rests on *the product of the two* small parameters: (i) the micro-to-macro ratio $1/TR$, and (ii) the viscosity-to-entropy ratio η/s. For central AA collisions, both are small or of order $\mathcal{O}(1/10)$. For high enough multiplicity of the pA and pp collisions, such as the first parameter becomes the same as in current AA collisions, the accuracy of hydrodynamics should be the same. While those value of multiplicity are not reached yet, hydrodynamics apparently starts to work, albight with less accuracy.

After solving the hydrodynamical equations we found that the *radial* (axially symmetric) flow is little modified by viscosity and is in fact enhanced by "longer" (in dimensionless time) run. Thus our main prediction is an *enhanced radial flow*. Its signatures – growing $m_\perp$ slopes with the particle mass, or growing proton-to-pion-ratio – are indeed confirmed by recent CMS and ALICE data. This happens in spite of the fact, that AA feezeout happens at smaller T_f than in pA.

We extensively studied various forms of viscous hydrodynamics, from NS to IS to resummation of gradients as la LS. In short, those grow from AA to pA to pp, but perhaps even in the last case they remain manageable. Higher harmonics are obviously more penalized by viscous corrections, especially of higher order, as each gradient goes with extra factor m. The role of those should be studied further elsewhere.

Finally let us comment the following: version 1 of this paper also included a view on the high multiplicity pp/pA from microscopic model, based on stringy Pomeron. It had grown substantially and will now appear as a separate publication.

Note added: When this version of the paper was completed, we learned about ALICE measurements of the identified particle spectra in high multiplicity pPb collisions [28]. Strong radial flow, growing with the multiplicity, is reported, clearly seen in proton/antiproton spectra. All conclusions are completely consistent with ours. Note especially one point: ALICE also finds that in pPb the freezeout happens at temperature $T_f^{pPb} \approx 0.17\,GeV$ higher than that in central PbPb, in which $T_f^{PbPb} \approx 0.12\,GeV$.

Acknowledgements. ES would like to thank former student Pilar Staig for her help in developing many of the ideas presently discussed. We also thank Gokce Basar, Dima Kharzeev and Derek Teaney for discussions. This work was supported by the U.S. Department of Energy under Contract No. DE-FG-88ER40388.

[1] E. Shuryak and I. Zahed, arXiv:1301.4470 [hep-ph].
[2] E. V. Shuryak, Phys. Lett. B **78**, 150 (1978) [Sov. J. Nucl. Phys. **28**, 408 (1978)] [Yad. Fiz. **28**, 796 (1978)].
[3] E. V. Shuryak and O. V. Zhirov, Phys. Lett. B **89**, 253 (1979).
[4] T. C. Brooks *et al.* [MiniMax Collaboration], Phys. Rev. D **61**, 032003 (2000) [arXiv:hep-ex/9906026].
[5] Observation of Long-Range, Near-Side Angular Correlations in Proton-Proton Collisions at the LHC, The CMS Collaboration, submitted to Journal of High Energy Physics, presented at CERN seminar Sept.21,2010.
[6] S. Chatrchyan *et al.* [CMS Collaboration], [arXiv:1210.5482 [nucl-ex]].
[7] B. Abelev *et al.* [ALICE Collaboration], arXiv:1212.2001 [nucl-ex].
[8] G. Aad *et al.* [ATLAS Collaboration], arXiv:1212.5198 [hep-ex].
[9] A. Adare *et al.* [PHENIX Collaboration],

[arXiv:1303.1794 [nucl-ex]].
[10] E. Shuryak, arXiv:1009.4635 [hep-ph].
[11] P. Bozek, Phys. Rev. C **85**, 014911 (2012) [arXiv:1112.0915 [hep-ph]].
[12] H. Marrochio, J. Noronha, G. S. Denicol, M. Luzum, S. Jeon and C. Gale, arXiv:1307.6130 [nucl-th].
[13] S. Chatrchyan *et al.* [CMS Collaboration], arXiv:1307.3442 [hep-ex].
[14] T. Pierog, I. .Karpenko, J. M. Katzy, E. Yatsenko and K. Werner, arXiv:1306.0121 [hep-ph].
[15] Z. W. Lin, Current status and further improvements of a multi-phase transport (AMPT) model, Indian J. Phys. 85 (2011) 837, doi:10.1007/s12648-011-0086-7.
[16] P. Romatschke, Int. J. Mod. Phys. E **19**, 1 (2010) [arXiv:0902.3663 [hep-ph]].
[17] B. B. Abelev *et al.* [ALICE Collaboration], arXiv:1307.6796 [nucl-ex].
[18] S. S. Gubser, Phys. Rev. D **82**, 085027 (2010) [arXiv:1006.0006 [hep-th]].
[19] S. S. Gubser and A. Yarom, Nucl. Phys. B **846**, 469 (2011) [arXiv:1012.1314 [hep-th]].
[20] M. Lublinsky and E. Shuryak, Phys. Rev. D **80**, 065026 (2009) [arXiv:0905.4069 [hep-ph]].
[21] P. Staig and E. Shuryak, Phys. Rev. C **84**, 034908 (2011) [arXiv:1008.3139 [nucl-th]].
[22] R. A. Lacey, Y. Gu, X. Gong, D. Reynolds, N. N. Ajitanand, J. M. Alexander, A. Mwai and A. Taranenko, arXiv:1301.0165 [nucl-ex].
[23] P. Staig and E. Shuryak, Phys. Rev. C **84**, 044912 (2011) [arXiv:1105.0676 [nucl-th]].
[24] G. Policastro, D. T. Son and A. O. Starinets, Phys. Rev. Lett. **87**, 081601 (2001) [hep-th/0104066].
[25] E. Shuryak, Phys. Rev. C **86**, 024907 (2012) [arXiv:1203.6614 [hep-ph]].
[26] M. P. Heller, R. A. Janik and P. Witaszczyk, Phys. Rev. Lett. **108**, 201602 (2012) [arXiv:1103.3452 [hep-th]].
[27] D. Teaney, Phys. Rev. C **68**, 034913 (2003) [nucl-th/0301099].
[28] B. B. Abelev *et al.* [ALICE Collaboration], arXiv:1307.6796 [nucl-ex].
[29] K. Dusling and R. Venugopalan, arXiv:1211.3701 [hep-ph]; arXiv:1210.3890 [hep-ph]; Phys. Rev. Lett. **108**, 262001 (2012) [arXiv:1201.2658 [hep-ph]].
[30] While the cost of an average "min.bias" *pp* collision is (number of events)/(cost of LHC)$\sim 10^{10}/10^{10}\$ = 1\$$, in the selected sample the cost is then about $10^6\$$/event.
[31] The reader may ask why not other series, such as e.g. leading to e^{-x}. While there is not enough known higher order terms to tell the difference, large x behavior of the geometric series seems to us more appropriate.
[32] This consideration has been proposed by D.Teaney in the discussion.